

In order to standardize the voxel spacing, the image was resampled to a voxel size of 1 mm × 1 mm × 1 mm. In addition, fixed discrete voxel intensity values with window width of 400–500 HU and window position of 20–50 HU are used to reduce image noise and normalized intensity and ensure that the processed images are at the same resolution (36–38). The image omics features are extracted from the segmented region of interest (ROI). These features can contain a wide range of data, including shape, intensity, texture, and band signs. This step converts visual information into quantifiable data that can be statistically analyzed (39–41). The geometric features describe the three-dimensional shape characteristics of ROI. Intensity characteristics describe the first-order statistical distribution of ROI voxel intensity. Texture features describe the second-order and higher-order spatial distribution patterns of intensity. The features extracted in this study include first order statistics (FOS), grey level co-occurrence matrix (GLCM), grey level run length matrix (GLRLM), grey level size zone matrix (GLSZM), neighbouring gray-tone difference matrix (NGTDM), gray level dependence matrix (GLDM) and morphological characteristics. Finally, the image omics features extracted from all patients were standardized by calculating the Z-value. A total of 1,834 imaging omics features were extracted from 3D segmentation of ROI for each patient.

The pre-trained model used in this study is Resnet50, and deep-learning features of each patient's AvgPool layer can be extracted from the trained Resnet50 model. 2,048 deep learning features can be extracted from each patient's AVgpool layer, and a total of 10,240 features can be extracted from 5 layers. Then principal component analysis (PCA) was used for data dimensionality reduction (42), and 4,000 deep learning features were obtained for each patient.

Results using the ResNet-50 pre-training model showed that in the training group, the area under the curve (AUC) value was 0.839 [95% confidence interval (CI): 0.8195–0.8579], the sensitivity was 0.753, and the specificity was 0.758, indicating that the model exhibited good predictive performance in this group. In contrast, in the validation group, the AUC value decreased to 0.646 (95% CI: 0.5967–0.6961), the sensitivity was 0.809, and the specificity was only 0.452 (Table S1). Although the results of the validation group did not meet the expected prediction performance, it still showed that ResNet-50 effectively captured the details and semantic information in the image in the training

group, reflecting its strong feature extraction capability.

The following three methods were used for feature screening for the extracted image omics and deep learning features. In the first step, portal hypertension and non-portal hypertension were grouped for the test, and features with $P < 0.05$ were screened. In the second walk correlation analysis, the threshold is set at 0.9 to reduce redundancy and further narrow the feature range by eliminating highly correlated variables. Finally, the minimum absolute contraction and selection operator (LASSO) regression model is used for feature screening on the training set. According to the adjustment weight λ , LASSO narrows all regression coefficients to zero and sets the coefficients for many unrelated features precisely to zero. In order to find the optimal λ , 10 cross-validations of the minimum criterion are used, where the final value of λ produces the smallest cross-validation error, and the feature that the coefficient is not 0 is preserved at the end (43,44).

References

36. Li M, Fan Y, You H, et al. Dual-Energy CT Deep Learning Radiomics to Predict Macrotrabecular-Massive Hepatocellular Carcinoma. *Radiology* 2023;308:e230255.
37. Sun R, Limkin EJ, Vakalopoulou M, et al. A radiomics approach to assess tumour-infiltrating CD8 cells and response to anti-PD-1 or anti-PD-L1 immunotherapy: an imaging biomarker, retrospective multicohort study. *Lancet Oncol* 2018;19:1180-91.
38. Han W, Qin L, Bay C, et al. Deep Transfer Learning and Radiomics Feature Prediction of Survival of Patients with High-Grade Gliomas. *AJNR Am J Neuroradiol* 2020;41:40-8.
39. Aerts HJ, Velazquez ER, Leijenaar RT, et al. Decoding tumour phenotype by noninvasive imaging using a quantitative radiomics approach. *Nat Commun* 2014;5:4006. Erratum in: *Nat Commun* 2014;5:4644.
40. Zhong X, Cao R, Shakeri S, et al. Deep transfer learning-based prostate cancer classification using 3 Tesla multi-parametric MRI. *Abdom Radiol (NY)* 2019;44:2030-9.
41. Srinivas C, K S NP, Zakariah M, et al. Deep Transfer Learning Approaches in Performance Analysis of Brain Tumor Classification Using MRI Images. *J Healthc Eng* 2022;2022:3264367.
42. Kumar V, Gu Y, Basu S, et al. Radiomics: the process and the challenges. *Magn Reson Imaging* 2012;30:1234-48.

43. Zhou M, Scott J, Chaudhury B, et al. Radiomics in Brain Tumor: Image Assessment, Quantitative Feature Descriptors, and Machine-Learning Approaches. *AJNR Am J Neuroradiol* 2018;39:208-16.

44. Avery E, Sanelli PC, Aboian M, et al. Radiomics: A Primer on Processing Workflow and Analysis. *Semin Ultrasound CT MR* 2022;43:142-6.

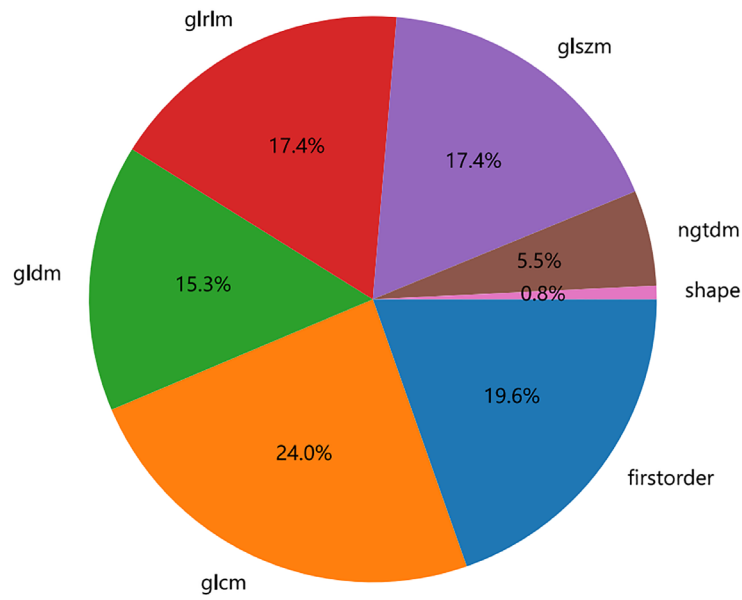


Figure S1 Radiomics features.

Table S1 Deep learning end-to-end predictive model performance evaluation

Group	Model	AUC	95% CI	Sensitivity	Specificity
Development cohorts	resnet50	0.839	0.8195–0.8579	0.753	0.758
Test cohorts	resnet50	0.646	0.5967–0.6961	0.809	0.452

AUC, area under the curve; CI, confidence interval.

Table S2 Characteristic parameters of the image omics model and their corresponding weighting coefficients

Variable (radiology feature parameters)	Coefficient
exponential_firstorder_Skewness	0.003182
exponential_glszm_ SmallAreaLowGrayLevelEmphasis	0.004797
exponential_ngtdm_Busyness	0.050271
lbp_3D_k_glrIm_RunEntropy	-0.003469
lbp_3D_m1_firstorder_RootMeanSquared	-0.00217
lbp_3D_m1_gldm_DependenceEntropy	-0.004816
lbp_3D_m2_glrIm_RunVariance	-0.004425
lbp_3D_m2_glrIm_ ShortRunHighGrayLevelEmphasis	0.006395
lbp_3D_m2_glszm_GrayLevelVariance	-0.006437
original_shape_Elongation	-0.003184
original_shape_Flatness	-0.00823
original_shape_SurfaceVolumeRatio	0.026454
squareroot_glcm_Correlation	-0.009418
wavelet_HHL_firstorder_Mean	0.006924
wavelet_HLH_ngtdm_Busyness	-0.010662
wavelet_HLL_firstorder_Range	-0.006052
wavelet_HLL_firstorder_Skewness	-0.010854
wavelet_HLL_glszm_ LowGrayLevelZoneEmphasis	0.00446
wavelet_LLL_glszm_ZoneEntropy	-0.00922
wavelet_LLL_glszm_ZoneEntropy	-0.00922
wavelet_LLL_ngtdm_Busyness	0.001817

Table S3 Feature parameters of the pre fusion model and their corresponding weighting coefficients

Variable	Coefficient
02DL_265	0.002309
02DL_329	0.001857
02DL_351	0.001053
02DL_428	0.002784
04DL_465	0.00018
04DL_688	0.005119
DL_0	-0.01261
DL_23	-0.000163
DL_230	-0.00076
_02DL_3	-0.017416
_02DL_5	-0.00268
_02DL_16	-0.006247
_02DL_298	-0.003437
_02DL_610	-0.000625
_02DL_628	-0.001139
_04DL_1	-0.03069
_04DL_3	-0.00303
_04DL_30	-0.002218
_04DL_143	-0.004628
exponential_ngtdm_Busyness	0.013897
lbp_3D_m2_glrIm_RunVariance	-0.008909